An intelligent system for reflow oven temperature settings based on hybrid physics-machine learning model

Yangyang Lai and Ke Pan
Department of Mechanical Engineering, Binghamton University, Binghamton, New York, USA
Yuqiao Cen
Department of Systems Science and Industrial Engineering, Binghamton University, Binghamton, New York, USA, and
Junbo Yang, Chongyang Cai, Pengcheng Yin and Seungbae Park
Department of Mechanical Engineering, Binghamton University, Binghamton, New York, USA

Abstract

Purpose – This paper aims to provide the proper preset temperatures of the convection reflow oven when reflowing a printed circuit board (PCB) assembly with varied sizes of components simultaneously.

Design/methodology/approach – In this study, computational fluid dynamics modeling is used to simulate the reflow soldering process. The training data provided to the machine learning (ML) model is generated from a programmed system based on the physics model. Support vector regression and an artificial neural network are used to validate the accuracy of ML models.

Findings – Integrated physical and ML models synergistically can accurately predict reflow profiles of solder joints and alleviate the expense of repeated trials. Using this system, the reflow oven temperature settings to achieve the desired reflow profile can be obtained at substantially reduced computation cost.

Practical implications – The prediction of the reflow profile subjected to varied temperature settings of the reflow oven is beneficial to process engineers when reflowing bulky components. The study of reflowing a new PCB assembly can be started at the early stage of board design with no need for a physical profiling board prototype.

Originality/value – This study provides a smart solution to determine the optimal preset temperatures of the reflow oven, which is usually relied on experience. The hybrid physics–ML model providing accurate prediction with the significantly reduced expense is used in this application for the first time.

Keywords Artificial neural network (ANN), Computational fluid dynamics (CFD), Support vector regression (SVR), Reflow soldering, Solder joints, Thermal profiling, Reflow

Paper type Research paper

1. Introduction

Reflow soldering is the most widely used process to attach surface mount components to printed circuit boards (PCBs). The process aims to form robust solder joints as the mechanical and electrical connections between the components and the PCB (Pan *et al.*, 2019). Properly developed the reflow profile can achieve defect-free solder joints by eliminating skewing, bridging, voiding, insufficient wetting, solder balling, tombstoning, dewetting, intermetallic compound excessiveness and other issues (Wang *et al.*, 2010; Xu *et al.*, 2020). However, the temperature profiles of solder joints under the components are hard to measure directly. Usually, process engineers collect temperature data using thermocouples attached to the surface of PCB or packages. For small size components, the measured surface temperature may reflect solder joint temperature approximately (Ha *et al.*, 2020; Shen *et al.*, 2005). But there is a large temperature deviation within bulky components. For big-size components, such as ball grid array (BGA) packages, the local temperatures of solder joints are lower than their surface temperatures. The temperature difference is determined by the component's thermal mass(Cai *et al.*, 2020). Hence, for large-size components, an accurate prediction for solder joint temperature is necessary. The minimum reflow temperature should be reached in these bulky components.

Numerical methods, such as the finite element method and finite volume method are widely used to obtain local solder temperature during the reflow soldering process. Shen conducted a finite element method simulation to investigate the solder temperatures of a BGA package (Shen *et al.*, 2005). Lai used the computational fluid dynamics (CFD) model to analyze the temperatures of solder balls of a BGA assembly during the reflow soldering process (Lai *et al.*, 2021). Shao used

The current issue and full text archive of this journal is available on Emerald Insight at: **https://www.emerald.com/insight/0954-0911.htm**

Soldering & Surface Mount Technology
34/5 (2022) 266–276

[DOI 10.1108/SSMT-10-2021-0063]

Received 2 October 2021
Revised 23 November 2021
Accepted 5 January 2022

the CFD model to obtain the working status temperature distribution of a 2.5 D package and mapped it to the finite element analysis model to observe component warpage (Shao *et al.*, 2018). Deng used the CFD model to predict the temperature distribution of a system in package assembly during the reflow soldering process (Deng *et al.*, 2014). To obtain the ideal profile, however, a huge computational cost is required because of the complex combination of boundary conditions. The complexity depends on how many zones the reflow oven has. Nowadays, reflow ovens with 6–12 heating zones are widely used to reflow lead-free PCB assemblies (Salam *et al.*, 2004). The flexibility of individual temperature settings for the top and bottom modules of each zone doubles the combination.

To reduce the computation cost, a hybrid physics–machine learning (ML) model is introduced in this paper. First, an automated system is programmed to generate command scripts that are readable by the CFD solver. Scripts with varied combinations of material properties and boundary conditions are transferred into the ANSYS FLUENT solver, which is used in this study. The solver controlled by the automated system is programmed to read scripts and export results sequentially. Then, the organized results will be fed to the ML model as the training data. Finally, support vector regression (SVR) and neural network (NN) are used to validate the accuracy of ML prediction.

In the past, artificial intelligence has been widely used to investigate the reflow process. Zhancheng used an SVM model to predict the real process temperature at any point on the PCB (Zhancheng *et al.*, 2006). Tsai and Yang (2005) used a neuro-computing approach to predict the second-side thermal profile of PCB assemblies. Lam (2020) presents a noncontact temperature prediction of PCB during the reflow process. However, those three works are based on field measurement data that does not capture the solder joint temperatures, which are the real interests of reflow profile development. Additionally, the training data provided to ML models requires a costly number of experiments. The hybrid method introduced in this paper uses numerical simulation replacing repetitive parts of the physical model with the ML model (Willard *et al.*, 2020). This method accurately reproduces the behavior of a physics model at substantially reduced computation cost.

In this study, the CFD model is validated by using measurement results. The surface temperatures of the component and PCB well match the simulation results with boundary condition independence considered. To improve computation efficiency, the compacting model method is present to eliminate the small and thin features within the package. A 45 × 45 mm BGA package is treated as the specimen of the temperature prediction. The hybrid physics–ML method is used to find out the relationship between the reflow profile and input variables (e.g. the material properties of the package and the preset temperature of the reflow oven). SVR and artificial NN (ANN) are used to play the role of ML models.

The SVR formulation and concepts used in this work are based on reviewing literature (Drucker *et al.*, 1997; Shehab *et al.*, 2021). SVR model is used to investigate the relationship between input and output data. Assume the training data set of (xi,yi) for $i = 1,\ldots,n$ while $xi \in R^n$, $yi \in R$. The general function of SVR estimation takes the form as:

$$f(x) = (\omega \cdot \varphi(x_i)) + b \tag{1}$$

where ω is a weighting matrix, b is a bias term, $\varphi(x)$ represents the high-dimensional feature spaces that are nonlinearly mapped from the input space (Ghorbani *et al.*, 2020). The coefficients ω and b are estimated by minimizing the regularized risk function:

$$\frac{1}{2} \parallel \omega^2 \parallel + C \sum_{\iota=1}^{n} (\xi_i + \xi_i^*) \tag{2}$$

subject to

$$\begin{cases} y_i - \omega \cdot \varphi(x_i) - b \leq \varepsilon + \xi_\iota \\ -y_i + \omega \cdot \varphi(x_i) + b \leq \varepsilon + \xi_\iota^* \quad \mathrm{i} = 1, \ 2, \ldots, \mathrm{n} \\ \xi_\iota, \ \xi_\iota^* \geq 0 \end{cases} \tag{3}$$

where ε is the permissible error, and C is a coefficient to determine the tradeoff between minimizing training errors and minimizing the model flatness. The vectors outside ε zone are controlled by slack variables ξ_i, ξ_i^*, which are introduced to accommodate unpredictable errors on the input training set. Using a kernel function, the required decision function can be expressed as:

$$f(x) = \sum_{\iota=1}^{n} (\alpha_i + \alpha_i^*) \cdot K(x_i, x) + b \tag{4}$$

The radial-basis function (RBF) as one of the kernels used in this study is expressed:

$$K(x_i, x) = \exp\left\{ -\frac{|x_i, x|}{\sigma^2} \right\} \tag{5}$$

where the σ is the kernel parameter.

The ANN model with the Levenberg–Marquardt (LM) algorithm is used to map the data sets of input and to the output (Moré, 1978). It is a feed-forward network with a sigmoid transfer function in the hidden layer and a linear transfer function in the output layer. The weighted data in nodes of each layer are summed with the added bias before moving to subsequent layers. The LM algorithm is an iterative technique for solving nonlinear least-squares problems and which is expressed as the sum of squares of nonlinear functions. It can be thought of as a combination of the steepest descent and the Gauss–Newton method (Adeloye and Munari, 2006).

2. Computational fluid dynamics model and validation

2.1 Model geometry and simulation results

The model of a PCB assembly with six identical BGA packages was constructed as shown in Figure 1. The board dimension is 110 × 120 × 1.6 mm. A 26 × 26 × 0.8 mm bare die is attached to the top of each substrate whose dimension is 30 × 30 × 0.5 mm. SAC305 (96.5Sn/3.0Ag/0.5Cu) solder was used as the interconnection between packages and PCB. The solder joint height is 0.4 mm with 0.8 mm pitch. The PCB assembly is in

Figure 1 Schematic of the CFD model

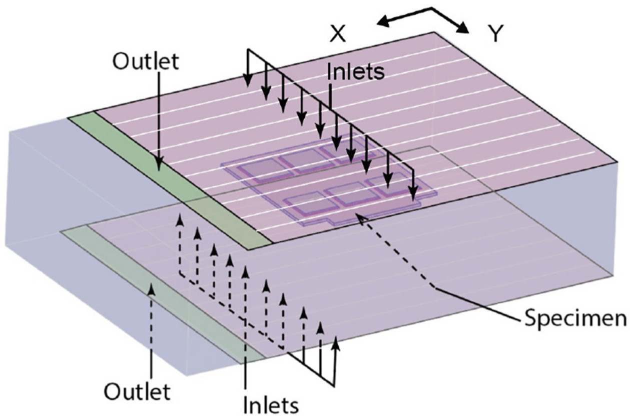

the center of the fluid domain, which appears semi-transparent. The y-axis in Figure 1 is the moving direction of the PCB assembly.

The geometry was transferred into a series of discrete control volumes using ANSYS-FLUENT. Since the solver is face-based, the polyhedral mesh is used for achieving more efficiency in comparison with tetrahedral or hybrid meshes. Mesh independence test was conducted for the solid and fluid domains, respectively (Lau *et al.*, 2012). To compare the solution stability of models with varied cell amounts, the surface temperatures of dies were selected as the monitor points. Peak temperature and time above liquidus (TAL) of the reflow profiles were the two parameters used to compare the variation of the results. At the same time, the residual error should be reduced to an acceptable value, typically 10^{-4} to 10^{-5}. The cell amount was finalized to 272,023.

Considering the movement of the PCB assembly during the reflow process, gas inlets are separated into ten groups with an individual temperature profile as the boundary condition. Each profile shares an identical trajectory but with an incremental delay time t_{delay} as shown in Figure 2. The delay time is associated with the conveyor speed v, and the spacing of each two adjacent inlets s_{inlet}, as shown in equation (1):

$$t_{delay} = n\ s_{inlet}\ /\ v \qquad (6)$$

By using this technique of boundary condition assignment, the dynamic thermal process was simulated by the CFD model as shown in Figure 3. The temperature gradient across the board in every time slot matches the realistic reflow environment, which is distinguished from the conventional simulations.

The transient model solver was used with pressure-based type and K-epsilon turbulence. The material property of the air was set in polynomial equations of temperature. The thermal properties of other items are listed in Table 1.

2.2 Experiment for validation

In this study, a six-zone forced convection oven is the reflow environment used. The PCB assembly goes through six heating zones and then one cooling zone sequentially. Three sets of the preset temperatures of six heating zones are shown in Table 2, which are used for the later validation work. The conveyor speed is 5.7 mm/s to reach a 300 s heating duration.

The specimen is a PCB assembly with six identical BGA packages as shown in Figure 4. A square bare die is on the top of each package. K-type thermocouples were attached to the center of each bare die. A thermal profiler was used to collect temperature data during the reflow process.

The surface temperatures of the PCB and six BGA packages were collected to compare with the results of the simulation. The variations of the six BGA temperatures and PCB temperatures at different locations are within 3°C. This indicates that the even temperature distribution in the x direction (Figure 1) is required in the numerical model. The simulation results of BGA package 1, 2 and 3 (Figure 4) were picked to show good agreement with the experimental results. Boundary condition independence was considered. The simulation results under three sets of boundary conditions (Table 2) well match experimental results as shown in Figure 5.

Figure 2 Temperature profiles for 10 inlets

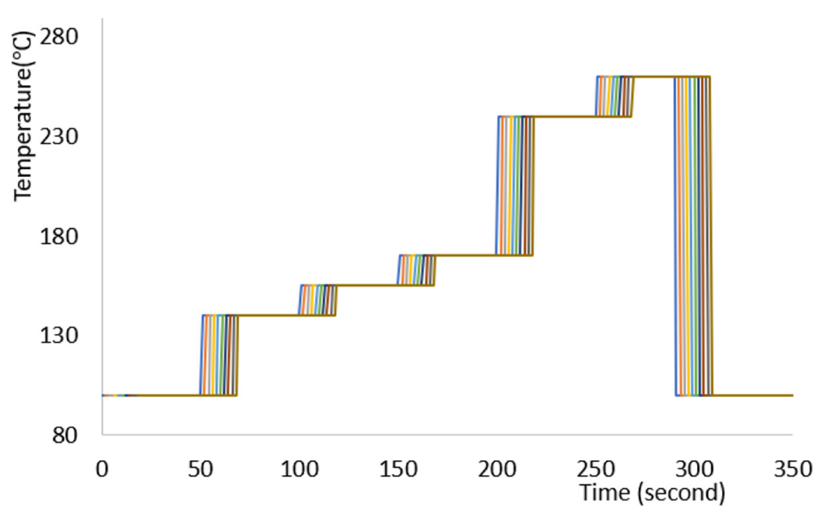

Figure 3 Temperature contours of PCB assembly from numerical simulation

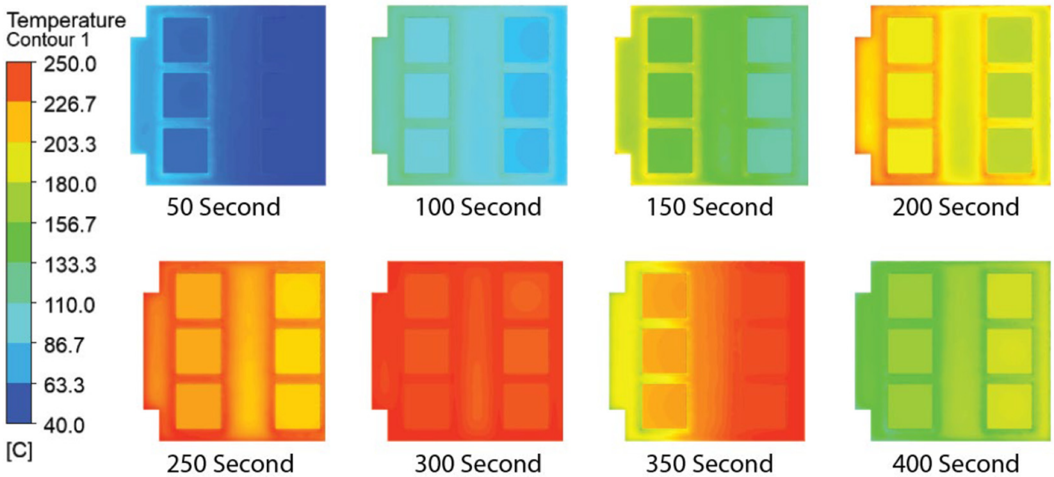

The difference at the peak temperature is 3.91°C. The maximum ramp rate difference is 1.34°C/s.

2.3 Compact model generation

Thin and small features such as C4, thermal interface material (TIM), and through silicon via make it impractical to use detailed models of microelectronic packages in board-level simulation (Pan *et al.*, 2021; Yang *et al.*, 2021). The compact model approach based on thermophysical property simplifications is used to eliminate these small features (Lasance, 2008).

The density and specific heat of lumped entities are recalculated by the following equation (7) and (8):

$$\rho_{eff} = \frac{\sum \rho_i V_i}{\sum V_i} \tag{7}$$

$$C_{eff} = \frac{\sum C_{p,i} m_i}{\sum m_i} \tag{8}$$

Based on the orientation of the materials of entities, heat conduction pathways can be identified as resistances in parallel and series directions. Orthotropic effective conductivities can be defined by the following equation (9) and (10):

$$K_{eff} = \sum \frac{K_i A_i}{A_{total}} \tag{9}$$

$$K_{eff} = \sum \frac{t_{total}}{\sum \frac{t_i}{K_i}} \tag{10}$$

A lidded BGA package is used as the specimen for the compact model study. Lidded packages are protected by a metal lid, which serves to spread the heat (Refai-Ahmed *et al.*, 2020). Three different simplification methods for lidded packages are presented in Figure 6. The detailed model serves as the reference for the error analysis. The performances of three different model simplifications are evaluated using equation (11) (Christiaens *et al.*, 1998):

$$Error = \frac{T_{compact} - T_{detail}}{T_{detail} - T_0} \tag{11}$$

Table 1 Material properties used for simulation

Material	*K* (W/m.K)	C_p (J/kg.K)	*d* (kg/m^3)
Air (27°C)	0.0263	1,007	1.1614
Air (77°C)	0.0300	1,009	0.9950
Air (127°C)	0.0338	1,014	0.8711
Air (177°C)	0.0373	1,021	0.7740
Air (227°C)	0.0407	1,030	0.6964
Air (277°C)	0.0439	1,040	0.6329
Silicon	98.4	721	2,300
PCB	0.2900	1,450	1,859
Sac305(solid)	$-0.007105.T + 70.52$	$0.22 + 0.00134.T\text{-}1642.T^2$	7,400
Sac305(liquidus)	25	259	8,000

Sources: Dusek *et al.* (2016), Yu *et al.* (2006)

Table 2 Temperature setting for heating zones

Zone	1	2	3	4	5	6
Temperature A (°C)	100	140	155	170	240	260
Temperature B (°C)	100	130	160	160	225	250
Temperature C (°C)	100	200	200	200	200	200

The error analysis testing is to heat components using 226.5°C impinging gas lasting 50 s. Terminal solder joint temperatures of four models are analyzed.

The error plot of compact models is shown in Figure 7. Only compact model C generates large errors that exceed the acceptable range, 5%(Lasance, 2008).

To minimize computation cost, the simplest model should be used once the error is within the safe range. From the result of the error analysis, the component should be separated into three portions. The upper part is the lid, which is above the core portion with die, C4, underfill, etc., lumped into a single block. The remaining part is the substrate on the bottom of the component.

3. Intelligent system

ANSYS-CORBA is used to perform client-server interactions with the connected ANSYS FLUENT as a server session. The code for coupling Python and ANSYS FLUENT is shown in Python-Fluent ANSYS as a server (AAS) coupling code. An intelligent system is programmed to generate command scripts that are readable for ANSYS FLUENT and to transfer them to ANSYS FLUENT as shown in Figure 8. The material properties (e.g. density, specific heat, thermal conductivity) of the lid, the core portion and the substrate are set as one group of the input factors. Copper and aluminum are used as two candidate materials for the lid. BT resin and ceramic are the two candidate materials for the substrate (Yang *et al.*, 2020). The core portion is a composite entity assigned three sets of material properties. Oven temperatures as another group of input factors contain four factors, corresponding to the preset

Figure 4 BGA packages and thermocouple attachment

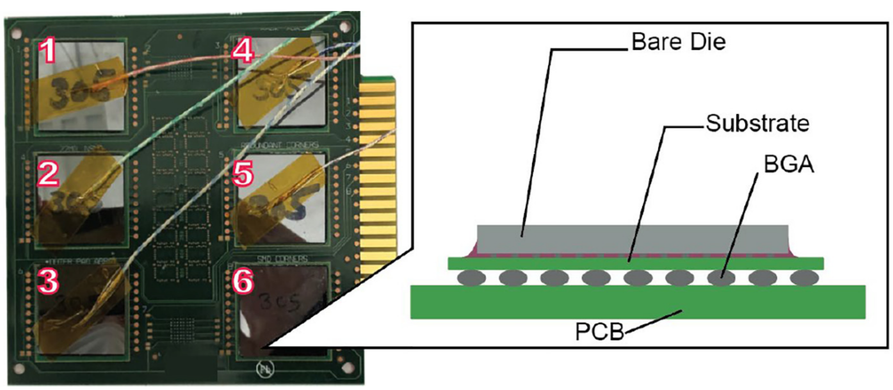

Figure 5 Comparison of the results of measurement and simulation for three BGA packages

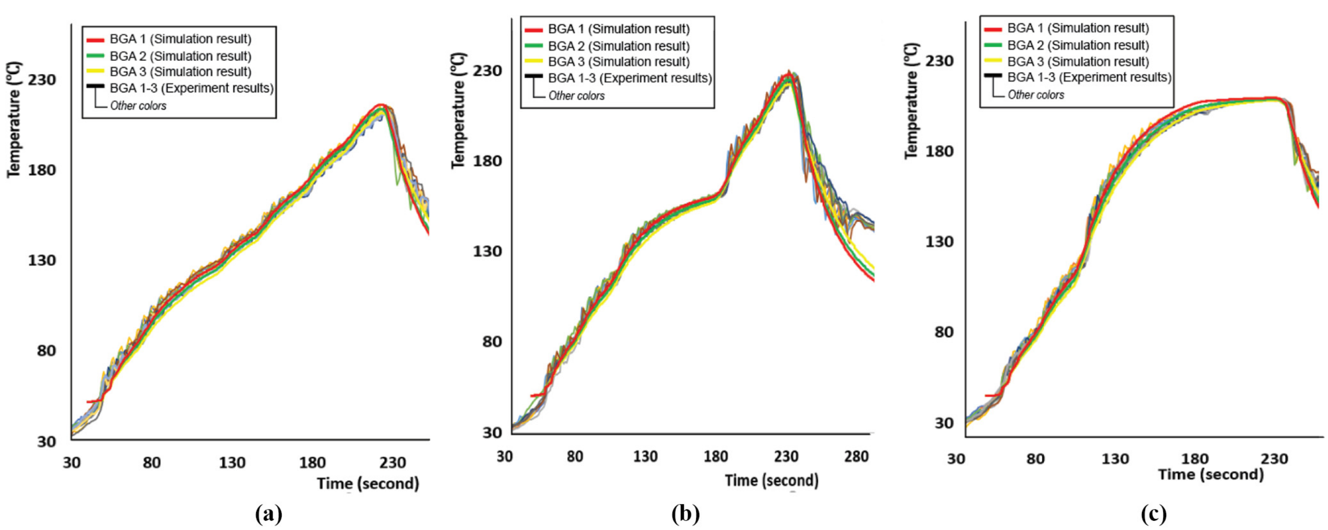

Notes: (a) Preset temperature A; (b) preset temperature B; (c) preset temperature C

Figure 6 Detailed model and compact models

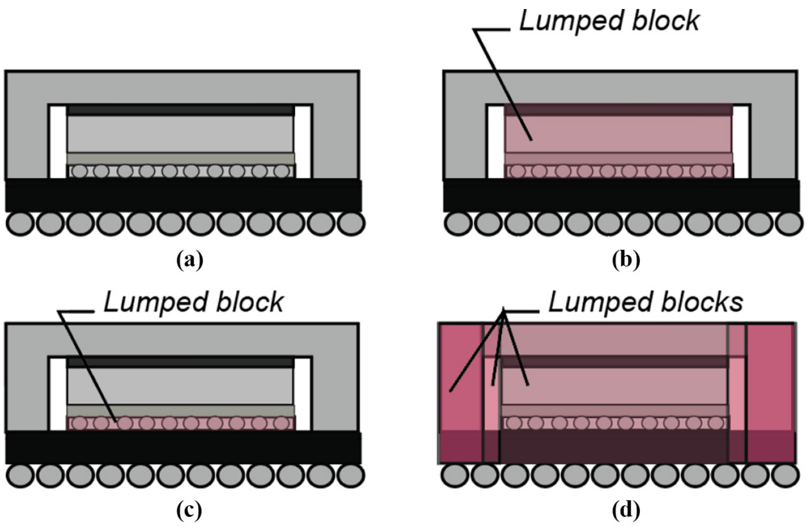

Notes: (a) Detailed model; (b) compact model A with lumped C4+underfill+die +TIM; (c) compact model B with lumped C4+underfill; (d) compact model C with 3 lumped blocks

temperature for Zone 3 to Zone 6. Two values are given to Zone 3 and Zone 6, while three values are given to Zone 4 and Zone 5 as shown in Table 3. The intelligent system generated 432 sets of input data and drove ANSYS FLUENT to solve them sequentially. After finishing the computing tasks, a comma-separated values file including input and output data was generated. The peak temperature and TAL of hot and cold spots are extracted as output data, which are the most significant factors for reflow profile assessment. Hot spots occur in the solder joints at the periphery of the package, whereas cold spots are at the center of the array or under the gap between the lid and die (Lau and Abdullah, 2013).

```
Python-Fluent AAS coupling code

os.chdir('D:\WorkingFolder')
import CORBA
import AAS_CORBA
```

Figure 7 Error plot of three compact models for lidded package

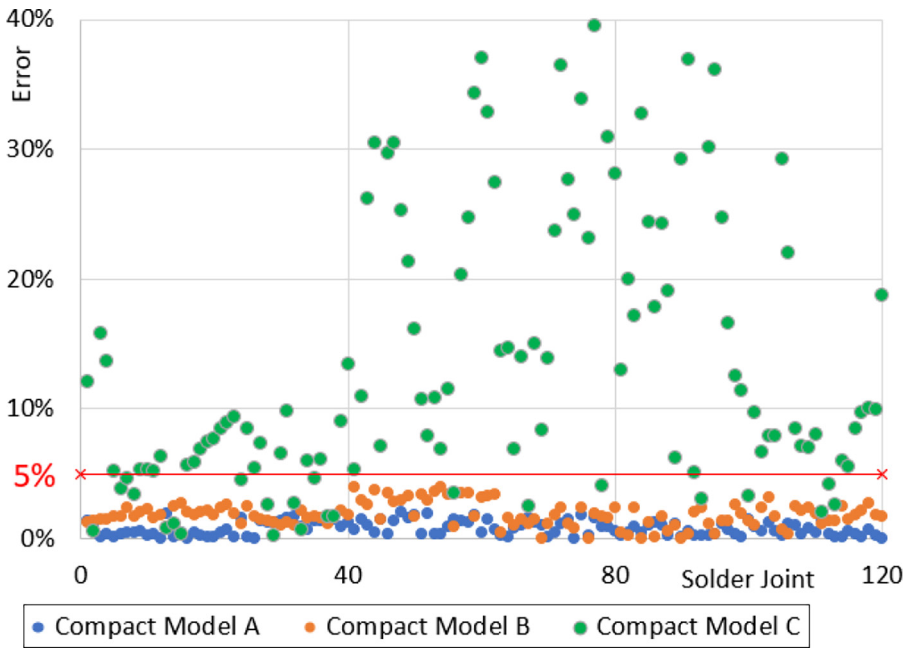

Figure 8 Flow chart of the intelligent system and hybrid physics-machine learning model

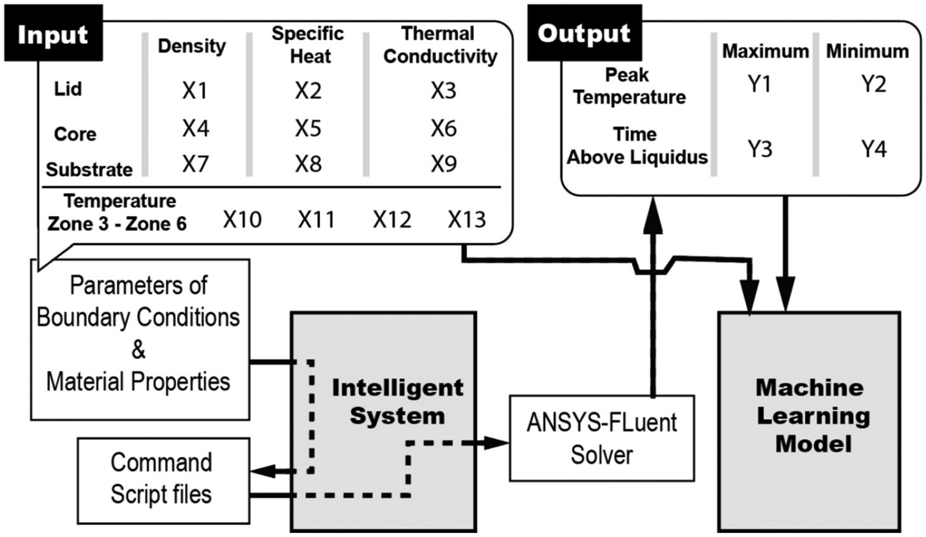


```
orb=CORBA.ORB_init()
with  open('aaS_FluentId.txt','r')  as  f:
aasFluentKey = f.read()

fluentUnit=orb.string_to_object
(aasFluentKey)
schemeController=fluentUnit.
getSchemeControllerInstance()

schemeController.doMenuCommand(Fluent  TUI
Command)
```

3.1 Machine learning model development

To develop the SVR models, two different kernel functions, namely, polynomial kernel function (Poly) and RBF were used. The SVR models were programmed in a python environment. A total of 80% of data sets were used for training. A total of 20% of the data sets were used to test the SVR model. Grid search and cross validation methodology were used to obtain the optimal parameters, i.e. *C*, *epsilon* and *d*.

The ANN with the Levenberg–Marquardt (LM) algorithm was used as the alternative ML model. The data were randomly divided into three sets. A total of 70% of data sets were used for training. A total of 15% of the data sets were used to validate the network is generalizing and to stop training before overfitting. The remaining 15% are used as a completely independent test of network generalization. If the network's performance is unsatisfying on the original data, more neurons should be added. If the performance on the training set is good, but the test set performance is worse, which could indicate overfitting, then reducing the number of neurons can improve results. If training performance is poor, then the number of neurons may have to increase. To get the least mean square error (MSE) and maximize computation efficiency, the number of hidden layers and the number of neurons were optimized by parametric testing (Ghorbani *et al.*, 2020). The ANN structure finally developed has a total of four layers with two hidden layers as shown in Figure 9.

The training time of the two models is within 5 s. The most consumption is the training data generation, which is highly dependent on the computer capability.

Table 3 Temperature setting for Zone 3–6

Zone	3	4	5	6
Temperature (°C)	150	170	210	250
	170	190	230	270
	NA	210	250	*NA*

3.2 Comparison of the results of support vector regression and artificial neural network

Statistical indices such as coefficient of determination (R^2) and MSE were used to evaluate the performance of the SVR and ANN models.

Table 4 shows the results based on two different kernels adopted in the SVR models. The RBF shows higher values of

Figure 9 Schematic of ANN architecture

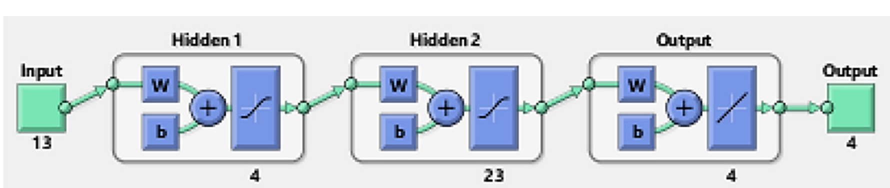

Table 4 Statistical evaluation of SVR models

	R2								MSE							
	Train				Testing				Train				Testing			
Output	Y1	Y2	Y3	Y4	Y1	Y2	Y3	Y4	Y1	Y2	Y3	Y4	Y1	Y2	Y3	Y4
SVR RBF	0.992	0.993	0.990	0.988	0.986	0.985	0.977	0.967	0.008	0.007	0.010	0.012	0.014	0.015	0.023	0.033
SVR Poly	0.973	0.950	0.942	0.905	0.952	0.888	0.877	0.822	0.027	0.050	0.058	0.095	0.048	0.112	0.123	0.178

Table 5 Statistical evaluation of ANN model

	Validate				Testing			
Output	Y1	Y2	Y3	Y4	Y1	Y2	Y3	Y4
R2	0.997	0.998	0.996	0.998	0.994	0.998	0.996	0.996
MSE	0.004	0.002	0.006	0.005	0.002	0.004	0.004	0.004

R^2 than the poly kernel and is used to compare with ANN performance later. Table 5 shows the prediction performance of ANN after dividing the data into the training, validating and test sets. Though there are only slight differences between the prediction results of ANN and SVR, the prediction using ANN is more accurate than SVR. No big difference is found between the performance of the test set and the training set, which proves overfitting does not exist.

The statistical indices including R^2 and MSE gave an overall view of the precision. To present the value of the error for the testing data sets, residual error graphs, which are the differences between the predicted and real output values are plotted in Figures 10 and 11, respectively. As presented in Figure 11, the data were almost equally scattered on both sides of the horizontal line for ANN models, which indicated the models do not underpredict or overpredict the peak temperature and TAL. The SVR model performs slightly worse in the symmetric aspect. For the prediction of peak temperature, there is no large difference between the SVR and ANN models. However, for TAL, the performance of the ANN model overwhelmed that of the SVR model.

4. Optimal preset temperature of each zone

Using the trained ML model, the peak temperature and TAL can be rapidly obtained with the input values. At the early stage

Figure 10 Residual error plots of SVR model

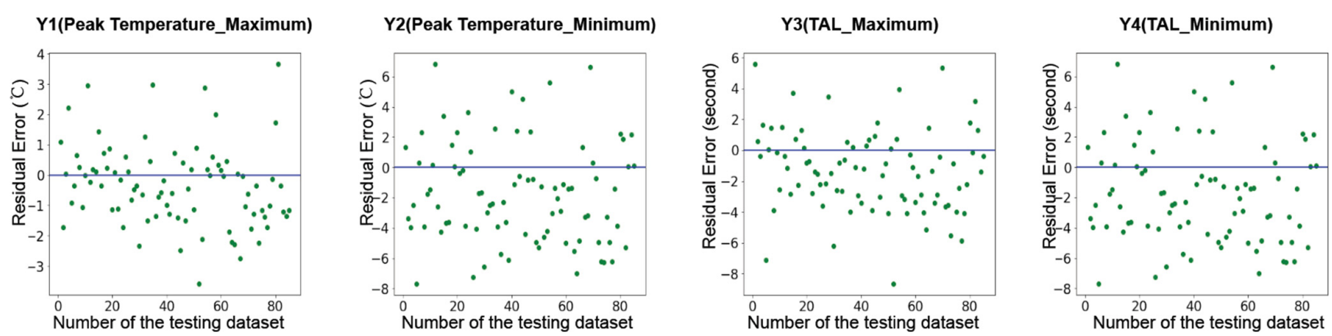

Figure 11 Residual error plots of ANN model

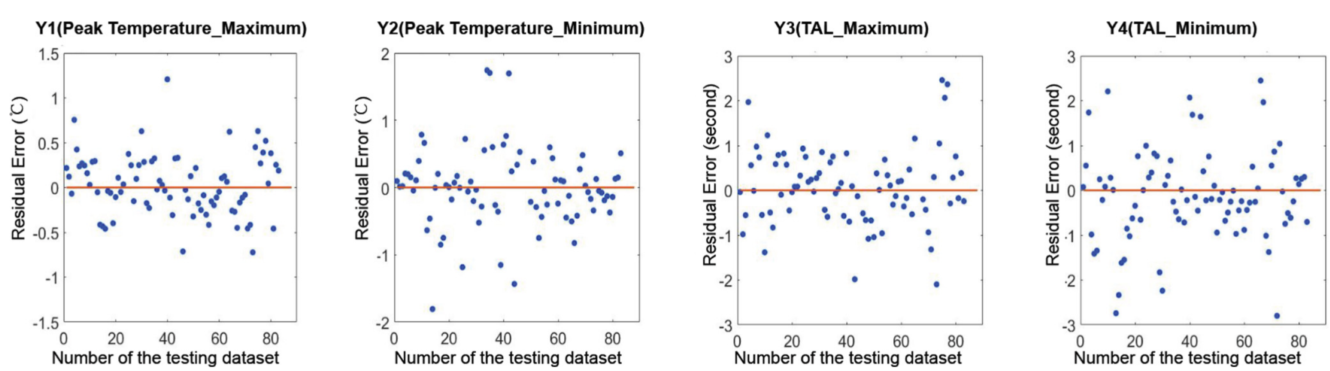

Figure 12 Flow chart of the optimal preset temperature

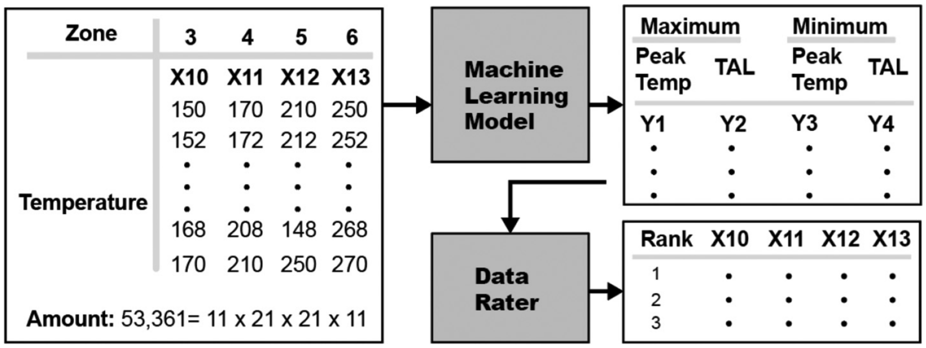

of board design, the reflow performance of a bulky component can be assessed effectively with the ML model instead of the costly numerical method. It also brings significant benefits to the reflow oven temperature setting job. In this study, the approach of the optimal preset temperatures is demonstrated using the trained ANN model.

As shown in Figure 12, 53,361 sets of preset temperatures are input to the ANN model. The corresponding 53,361 output data sets can be obtained in seconds. A data rater is used to filter, sort and rate the outputs and finally export the three optimal sets of preset temperatures.

Two criteria are used to filter the unqualified data sets. The minimum peak temperature (Y_3) should reach 230°C at least. The minimum TAL (Y_4) should reach 60 s at least. Both two criteria must satisfy before moving forward to the data sorting process. This step is to ensure minimum reflow temperature is reached for the cold spot.

The remaining data sets will be sorted by the maximum of peak temperature (Y_1) and TAL (Y_2) in ascending order. R_1 and R_2 are the order of data sets sorted by Y_1 and Y_2, respectively. This step is to sort out the lowest maximum temperature, which may impact the small and heat sensitive components.

R3, the order of data sorted by the increment of adjacent zones is introduced to evaluate the impact of thermal shock. Impact indexes I_1, I_2 and I_3 are used to assign the weight of each parameter as shown in Table 6. The optimal preset temperatures are ranked by the score calculated by the following equation (12):

$$Score = I_1 * R_1 + I_2 * R_2 + I_3 * R_3 \tag{12}$$

2, 1, and 0.5 are assigned to I_1, I_2, and I_3, respectively. The magnitude of the impact index indicates the corresponding impact to the reflow profile. These three values used here are for reference only.

Table 6 Impact index

Index	Parameter	Effect
I_1	Peak temperature	Damage small component
I_2	Time above liquidus	
I_3	Zone temperature slope	Thermal shock

After picking out the data sets with the lowest score, the corresponding input X_{10} to X_{13} are the optimal preset temperature of Zone 3 to Zone 6.

5. Conclusions

This paper presents a cost-effective method to determine reflow oven settings to achieve the desired reflow profile of a BGA package. The CFD model simulating the reflow soldering process was validated using the experiment results. An intelligent system was developed to connect the CFD model with the script generator. Using this programmed system, reflow profiles subjected to multiple sets of boundary conditions and material properties were collected and transferred to the ML model as training data sets. Two AI methods including ANN and SVR were used for predicting reflow profiles. The peak temperature and TAL of both hot and cold spots are regarded as the output of the model. The 0.96 above R^2 of the SVR and ANN models indicated the good performance in prediction. In comparison with SVR, ANN obtained better accuracy in TAL prediction. The optimal preset temperatures of the reflow oven were reversely obtained after evaluating tens of thousands of data sets output by the trained ML model in seconds. The high efficiency is the charm of the ML model in comparison to the costly numerical method. The ML model should be retrained for different components, and this can be conducted at the early stage of board design with no need for a profiling board.

This hybrid method integrating both physical and ML models synergistically can accurately predict reflow profiles of solder joints and alleviate the expense of repeated trials. The impact of material properties on reflow profile can be a good quantitative reference in the early stage of package design. The prediction of the reflow profile subjected to varied reflow oven preset temperatures can be obtained rapidly. The optimal preset solution obtained reversely is beneficial to the small volume production of complex PCB assembly.

References

Adeloye, A.J. and Munari, A. D. (2006), "Artificial neural network based generalized storage-yield-reliability models using the Levenberg-Marquardt algorithm", *Journal of Hydrology*, Vol. 326 Nos 1/4, pp. 215-230, available at: https://doi.org/10.1016/j.jhydrol.2005.10.033

Cai, C., Pan, K., Yang, J. and Park, S. (2020), "Comparative analysis of package warpage using confocal method and digital image correlation", *InterSociety Conference on Thermal and Thermomechanical Phenomena in Electronic Systems, ITHERM*, pp. 945-949, doi: 10.1109/ITherm45881.2020.9190235.

Christiaens, F., Vandevelde, B., Beyne, E., Mertens, R. and Berghmans, J. (1998), "Generic methodology for deriving compact dynamic thermal models, applied to the PSGA package", *IEEE Transactions on Components, Packaging, and Manufacturing Technology: Part A*, Vol. 21 No. 4, pp. 565-576, doi: 10.1109/95.740049.

Deng, S.S., Hwang, S.J. and Lee, H.H. (2014), "Thermal simulation of system in package (SiP) in soak zone of reflow process", *9th International Microsystems, Packaging, Assembly and Circuits Technology Conference: Challenges of Change – Shaping the Future, IMPACT 2014 – Proceedings, Institute of Electrical and Electronics Engineers Inc.*, pp. 238-241, doi: 10.1109/IMPACT.2014.7048402.

Drucker, H., Surges, C.J.C., Kaufman, L., Smola, A. and Vapnik, V. (1997), "Support vector regression machines", *Advances in Neural Information Processing Systems*, Vol. 5, pp. 155-161.

Dusek, K., Stancu, C., Notingher, P. V., Mach, P. and Placek, M. (2016), "Experimental and numerical analysis of melting and solidification of SnAgCu joints", *IEEE Transactions on Components, Packaging and Manufacturing Technology*, Vol. 6 No. 9, pp. 1445-1455, doi: 10.1109/TCPMT.2016.2593709.

Ghorbani, B., Arulrajah, A., Narsilio, G. and Horpibulsuk, S. (2020), "Experimental investigation and modelling the deformation properties of demolition wastes subjected to freeze–thaw cycles using ANN and SVR", *Construction and Building Materials*, Vol. 258, available at: https://doi.org/10.1016/j.conbuildmat.2020.119688

Ha, J., Pan, K., Wang, H., Won, D.H. and Park, S.B. (2020), "The effect of misaligned passive component on fatigue life of solder joints and solder shape", *InterSociety Conference on Thermal and Thermomechanical Phenomena in Electronic Systems, ITHERM*, pp. 1029-1034, doi: 10.1109/ITherm45881.2020.9190328.

Lai, Y., Pan, K., Xu, J., Yang, J. and Park, S. (2021), "Determination of smarter reflow profile to achieve a uniform temperature throughout a board", *InterSociety Conference on Thermal and Thermomechanical Phenomena in Electronic Systems, ITHERM*, pp. 911-916, doi: 10.1109/ITherm51669.2021.9503258.

Lam, T.L. (2020), "Low-cost non-contact PCBs temperature monitoring and control in a hot air reflow process based on multiple thermocouples data fusion", *IEEE Access*, Vol. 9, pp. 1-10, doi: 10.1109/ACCESS.2020.3036527.

Lasance, C.J.M. (2008), "Ten years of boundary-condition-Independent compact thermal modeling of electronic parts: a review", *Heat Transfer Engineering*, Vol. 29 No. 2, pp. 149-168, available at: https://doi.org/10.1080/01457630701673188

Lau, C.-S. and Abdullah, M.Z. (2013), "Simulation investigations on fluid/structure interaction in the reflow soldering process of board-level BGA packaging", *International Journal of Computer Theory and Engineering*, Vol. 1, pp. 645-649.

Lau, C.S., Abdullah, M.Z. and Ani, F.C. (2012), "Computational fluid dynamic and thermal analysis for BGA assembly during forced convection reflow soldering process", *Soldering & Surface Mount Technology*, Vol. 24 No. 2, pp. 77-91, available at: https://doi.org/10.1108/09540911211214659

Moré, J.J. (1978), "The Levenberg-Marquardt algorithm: Implementation and theory", Springer, Berlin, Heidelberg. pp. 105-116.

Pan, K., Xu, J., Lai, Y. and Park, S. (2021), "Investigation of copper and glass interaction in through glass via (TGV) during thermal cycling", *Electronic Components and Technology Conference*, IEEE, pp. 1660-1666, doi: 10.1109/ECTC32696.2021.00263.

Pan, K., Ha, J.H., Wang, H.Y., Veeraraghavan, V. and Park, S. B. (2019), "The effect of solder paste volume on surface mount assembly self-alignment", *Procedia Manufacturing*, Vol. 38, pp. 1381-1393, available at: https://doi.org/10.1016/j.promfg.2020.01.150.

Refai-Ahmed, G., Wang, H., Ramalingam, S., Karunakaran, N., Pan, K., Park, S.B. and Soundarajan, A. (2020), "Lidless and lidded flip chip packages for advanced applications", *IEEE 22nd Electronics Packaging Technology Conference, EPTC 2020*, doi: 10.1109/EPTC50525.2020.9315021.

Salam, B., Virseda, C., Da, H., Ekere, N.N. and Durairaj, R. (2004), "Reflow profile study of the Sn-Ag-Cu solder", *Soldering & Surface Mount Technology*, Vol. 16 No. 1, pp. 27-34, available at: https://doi.org/10.1108/09540910410517022

Shao, S., Niu, Y., Wang, J., Liu, R., Park, S., Lee, H. and Refai-Ahmed, G. (2018), "Comprehensive study on 2.5D package design for board-level reliability in thermal cycling and power cycling", *Proceedings – Electronic Components and Technology Conference*, Institute of Electrical and Electronics Engineers Inc., pp. 1668-1675, doi: 10.1109/ECTC.2018.00251.

Shehab, M., Alshawabkah, H., Abualigah, L. and Al-Madi, N. (2021), "Enhanced a hybrid moth-flame optimization algorithm using new selection schemes", *Engineering with Computers*, Vol. 37 No. 4, pp. 2931-2956, available at: https://doi.org/10.1007/s00366-020-00971-7

Shen, L., Wang, M., He, Y.H., Lam, T.F. and Jiang, Y.Q. (2005), "Reflow profile simulation by finite element method for a BGA package", *6th International Conference on Electronics Packaging Technology*, pp. 6-9, doi: 10.1109/ICEPT.2005.1564717.

Tsai, T.N. and Yang, T. (2005), "A neuro-computing approach to the thermal profile control of the second-side reflow process in surface mount assembly", *Journal of Manufacturing Technology Management*, Vol. 16 No. 3, pp. 343-359.

Wang, Y., Cui, Z. and Wang, B. (2010), "Test and assessment of the heating system of reflow ovens", *Proceedings – 2010 11th International Conference on Electronic Packaging Technology and High Density Packaging, ICEPT-HDP 2010*, pp. 798-804, 10.1109/ICEPT.2010.5582693.

Willard, J., Jia, X., Xu, S., Steinbach, M. and Kumar, V. (2020), "Integrating physics-based modeling with machine learning: a survey", Vol. 1 No. 1, pp. 1-34.

Xu, J., Cai, C., Pham, V., Pan, K., Wang, H. and Park, S. (2020), "A comprehensive study of electromigration in lead-free solder joint", *Proceedings – Electronic Components and Technology Conference*, pp. 284-289, doi: 10.1109/ECTC32862.2020.00054.

Yang, J., Xu, J. and Park, S. (2020), "Identification of polymer materials in electronic packages including counterfeit prevention", *Proceedings – Electronic Components and Technology Conference*, pp. 2317-2324, doi: 10.1109/ECTC32862.2020.00361.

Yang, J., Lai, Y., Pan, K., Xu, J., Mikjaniec, T., Cain, S. and Park, S. (2021), "A comparison study of TIM degradation of phase change material and thermal grease", *Electronic Components and Technology Conference*, *IEEE*, pp. 1978-1983.

Yu, H., Mattila, T.T. and Kivilahti, J.K. (2006), "Thermal simulation of the solidification of lead-free solder interconnections", *IEEE Transactions on Components and Packaging Technologies*, Vol. 29 No. 3, pp. 475-485, doi: 10.1109/TCAPT.2005.848590.

Zhancheng, W., Weimin, L., Hang, T. and Yangsheng, X. (2006), "A novel on-board temperature monitoring approach in the reflow soldering process", *IEEE International Conference on Intelligent Robots and Systems*, pp. 4245-4251, doi: 10.1109/IROS.2006.281952.

Corresponding author

Yangyang Lai can be contacted at: ylai9@binghamton.edu